



Full Length Article

Hierarchically synthesis of M@CeO₂ (M = Ba, Er) nanoparticles for Antibacterial efficacyK. Loganathan^{a,*}, R.P. Suresh Jeyakumar^b, Natarajan Arumugam^c,
Sinouvassane Djearmane^{d,e,*}, lingshing wong^{f,h}, Saminathan Kayarohanam^g^a Department of Chemistry, Vivekananda College of Arts and Sciences for Women (Autonomous) Elayampalayam, 637 205 Tamilnadu, India^b Department of Chemistry, K.S.Rangasamy College of Arts and Science (Autonomous) Tiruchengode, 637211, Tamilnadu, India^c Department of Chemistry, College of Science, King Saud University, P.O. Box 2455, Riyadh 11451, Saudi Arabia^d Department of Allied Health Sciences, Faculty of Science, University Tunku Abdul Rahman, Jalan University, Bandar Barat, Kampar 31900, Malaysia^e Biomedical Research Unit and Lab Animal Research Centre, Saveetha Dental College, Saveetha Institute of Medical and Technical Sciences, Saveetha University, Chennai 602 105, India^f Faculty of Health and Life Sciences, INTI International University, Nilai 71800 Malaysia^g Faculty of Bioeconomics and Health Sciences, University Geomatika Malaysia, Kuala Lumpur 54200, Malaysia^h School of Nursing, Shinawatra University, 99, Moo 10, Bangtoey, Samkhok, Pathum Thani 12160, Thailand

ARTICLE INFO

Keywords:

CeO₂ NPsBa / Er @ CeO₂ NPs

Co-precipitation method

SEM/EDX

ABSTRACT

Cerium oxide fine particles injected with metallic nanoparticles were produced using the co-precipitation method and characterized using various techniques such as XRD, SEM, FTIR, UV-Vis, and PL. Both injected and non-doped ceria nanoparticles exhibited a crystallographic structure similar to calcium fluoride. The nanoparticles ranged in size from 25 to 74 nm and had an inconsistent spherical shape. EDX analysis confirmed the presence of Erbium (Er) and Barium (Ba) in the ceria nanocrystal lattices. UV-Vis experiments showed that the optical band gap efficiency of purified CeO₂ NPs was 3.1 eV, while doped CeO₂ NPs had an energy level of 2.9 eV. The nanoparticles exhibited a sharp emission peak at approximately 347 nm. The synthesized CeO₂ NPs showed antibacterial activity against Gram-positive and Gram-negative bacteria, including *Bacillus subtilis*, *Staphylococcus aureus*, *Escherichia coli* and *Pseudomonas aeruginosa*. Overall, the results demonstrate that the doping of ceria nanoparticles with metallic nanoparticles can significantly enhance their antibacterial properties. This research paves the way for the development of novel antibacterial agents with potential applications in various fields such as medicine, food packaging, and water treatment.

1. Introduction

A large number of bacteria are present in our daily living environment, and the uncontrolled growth and spread of pathogenic bacteria can cause several human diseases and wound infections (Kumar et al., 2014). The discovery of penicillin has enabled humans to defend themselves against bacteria to some extent, and the extensive application of antibiotics has made a significant contribution to society. However, due to the heavy use of antibiotics, a high number of resistant bacteria strains have developed (Kumar et al., 2021), and the emergence of such drug-resistant bacteria has left traditional antibiotics inadequate in destroying them; hence, developing new antimicrobial agents to treat

bacteria is urgently required. A promising alternative to combat bacterial resistance comes from metal oxide nanoparticles (NPs). Metal oxide NPs have high chemical and biological activity due to different factors, mainly their small size and their high surface-to-volume ratio. As a result, they have been widely used in biology and medicine.

Genuinely, Cerium oxide (CeO₂) nanoparticles have an emerged as an exciting emerging substance with potential applications in therapeutics and electroluminescent technologies (Pelletier et al., 2010; Alpaslan et al., 2017). Among the many applications of nanostructured CeO₂-based composites in ecological and energy technology includes outgas cleansing, fuel cells made of solid oxide, oxygen gases detectors, electrochromic components, ultraviolet (UV) protective coatings, and

* Corresponding authors at: Department of Chemistry, Vivekananda College of Arts and Sciences for Women (Autonomous) Elayampalayam, 637 205 Tamilnadu, India (K. Loganathan). Department of Allied Health Sciences, Faculty of Science, University Tunku Abdul Rahman, Jalan University, Bandar Barat, Kampar 31900, Malaysia (S. Djearmane).

E-mail addresses: drkloganathan@vicas.org (K. Loganathan), sinouvassane@utar.edu.my (S. Djearmane).

<https://doi.org/10.1016/j.jksus.2024.103222>

Received 4 February 2024; Received in revised form 7 April 2024; Accepted 21 April 2024

Available online 23 April 2024

1018-3647/© 2024 The Author(s). Published by Elsevier B.V. on behalf of King Saud University. This is an open access article under the CC BY-NC-ND license (<http://creativecommons.org/licenses/by-nc-nd/4.0/>).

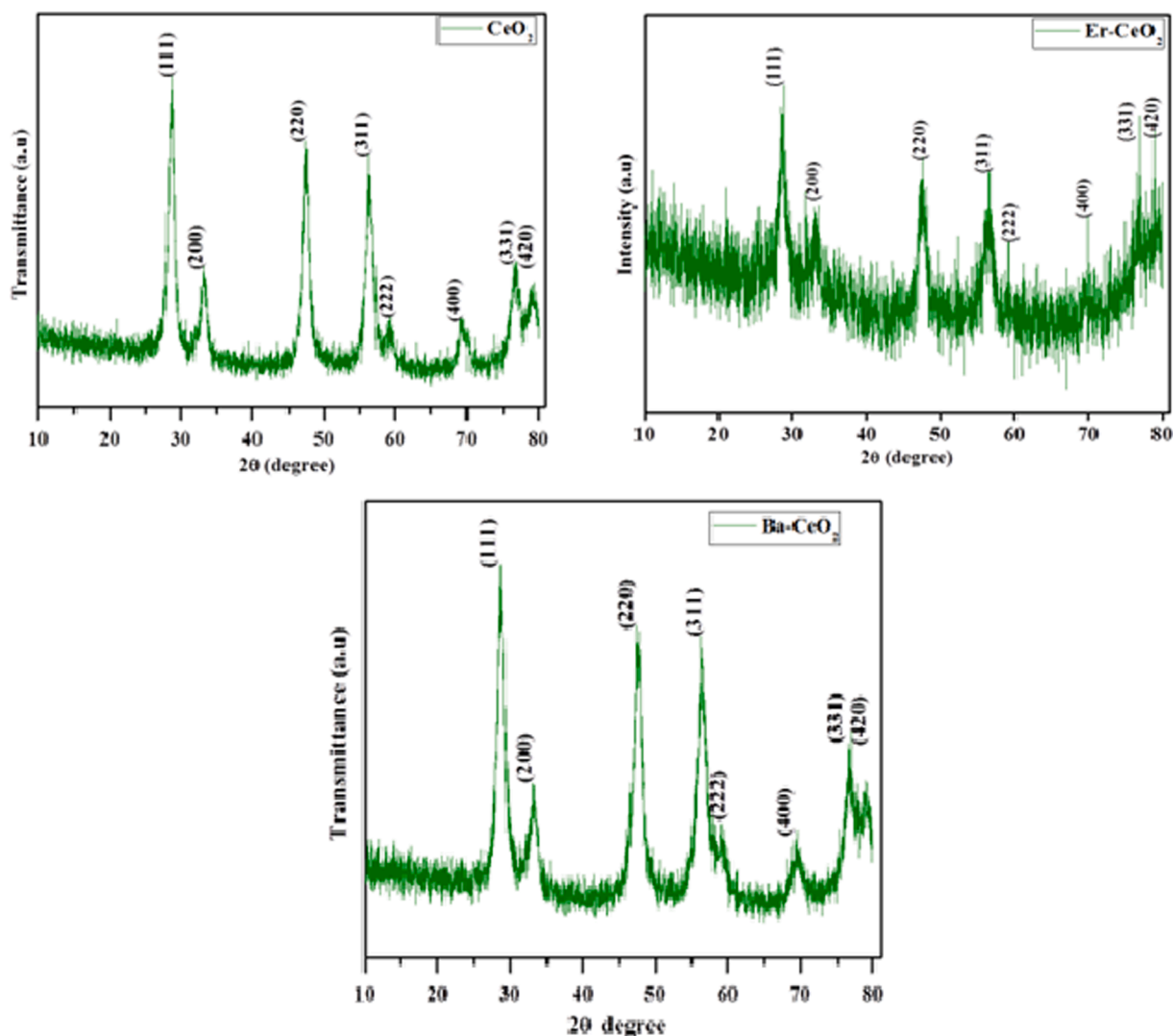


Fig. 1. XRD pattern of (a) Pristine CeO_2 (b) Er doped CeO_2 (c) Ba doped CeO_2 NPs.

electrochromic devices (Farias et al., 2018). According to oxygen shortages in the crystal structure of either pristine or loaded ceria are associated with the distinctive features of cerium dioxide. Modern study has concentrated on transistor photo catalysis, with TiO_2 being a popular photographic catalyst for waste from agriculture and industries due to its good characteristics (Malleshappa et al., 2015). According to, the band gap interaction between visible light, non-metallic the addition of doping and the photocatalyst's catalytic function and the movement of photo-induced pairs of electron-holes from the catalyst's interior to its exterior being narrowed (Cuahtecontzi-Delint et al., 2013). Therefore, doping of cerium oxide nanostructures improves their chemical and thermal stability, high ionic conductivity, and better UV absorption. The numerous reports of doping of various metals such as Co, Mg, Cd, Fe, Ni, Ag, and Zn with CeO_2 nanoparticles have been presented that are associated with improving the properties of new nanostructures. The erbium particles employed in optoelectronic cores for converting the energy of captured infrared rays into visible wavelengths are hosted inside the low-phonon material ceria (Khadar et al., (2019,)).

With the addition of alkaline metals onto the surfaces of CeO_2 matrices, which can change the optical and biocidal properties of nanomaterials, due to bandgap illumination, the electrons (e) of NMs are excited via the bandgap to the conduction band, producing holes (h^+) in the valence band. As a result, the conduction band electrons and the valence band holes produce highly active reducing and oxidizing agents.

These oxidizing agents (OH^- and O_2) are responsible for the antibacterial activity of CeO_2 NPs, which could be altered by doping the CeO_2 NPs with alkali metal ions (AMIs) because they (Ba ions) act as electron traps that can inhibit the rate of (e^-/h^+) pair recombination by augmenting the bandgap energy (Nithya and Sundrarajan, 2020). This stimulates the formation of ROS and increases the antibacterial efficacy. Therefore, the main objective of this research is to develop and compare the results of pristine and injected CeO_2 nanoparticles through precipitation approach employing polyethylene glycol (PEG) as a surfactant.

Experimental

Materials

Cerium nitrate hexahydrate ($\text{Ce}(\text{NO}_3)_3 \cdot 6\text{H}_2\text{O} > 99.8\%$), Erbium nitrate hexahydrate ($\text{ErH}_{12}\text{N}_3\text{O}_{15} > 99.9\%$) and Barium nitrate pentahydrate ($\text{BaH}_2\text{N}_2\text{O}_5 > 98.9\%$) were procured from sigma Aldrich, India. And bacterial strains were obtained from the microbial collection of the microbiology laboratory of Bharathidasan University, Tamilnadu, India. All the chemicals and reagents were used as AR grade. The whole experiment used as deionized water and without further sanitation.

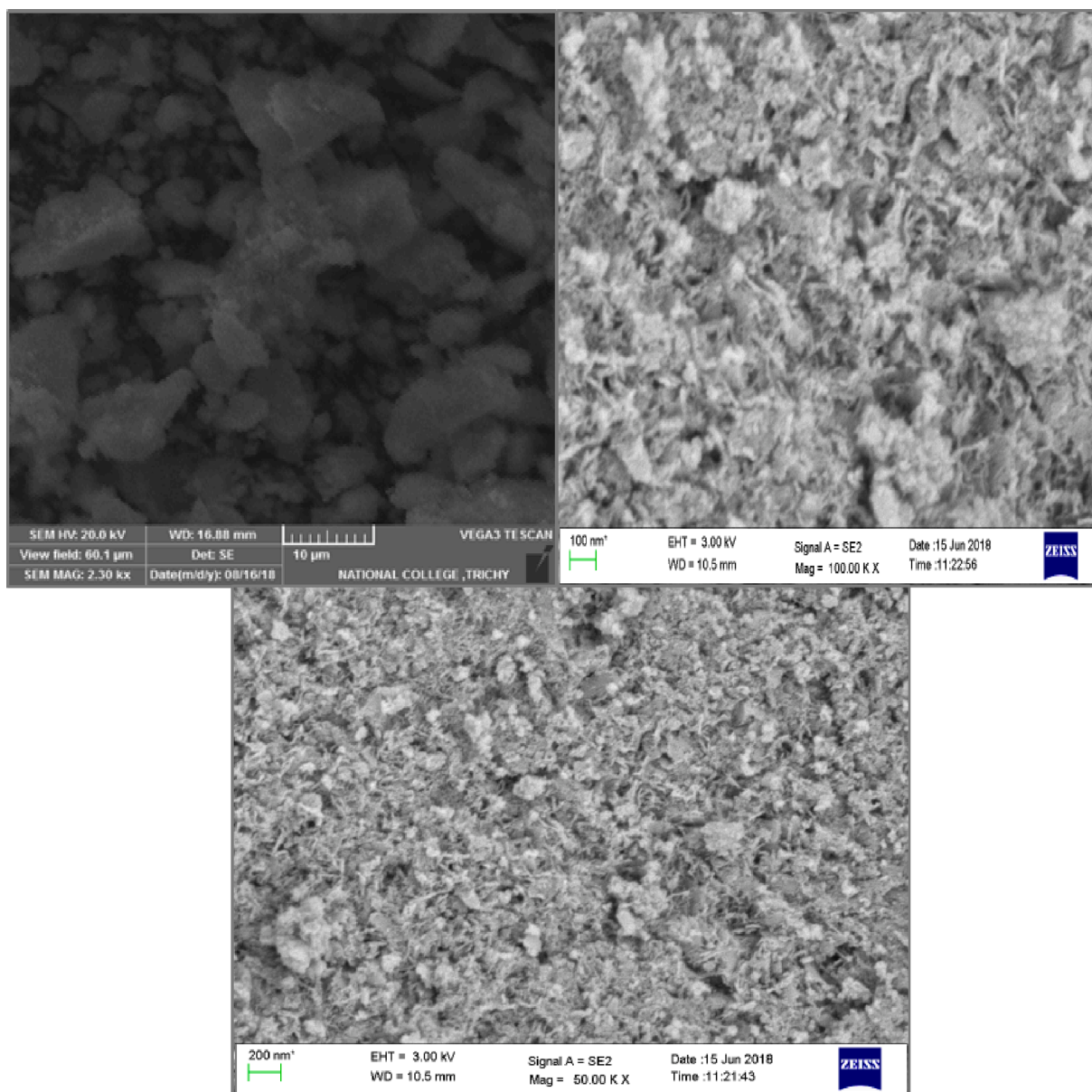


Fig. 2. SEM photograph of (a) Pristine CeO₂ (b) Er doped CeO₂ (c) Ba doped CeO₂ NPs.

1.1. Hierarchically fabrication of pristine M CeO₂ (M = Ba, Er) nanoparticles

Following dissolving 0.095 mg of cerium nitrate hexahydrate, 0.005 mg of Erbium nitrate hexahydrate, along with 0.8 mg of sodium hydroxide in their respective choices, the first step was to evenly combine the two solutions. The polyethylene glycol (PEG), which can function as a surfactant, is injected into the resultant combination mentioned earlier and subsequently lowered by a NaOH solution, resulting in a transparent yellow precipitate. After mixing the solution including the light-yellow precipitate for thirty minutes at the surrounding temperature, it was heated to 60 °C and fed for a total of four hours. After one day at a reasonable humidity, the combination of reaction fluid was refluxed to provide a clear solution. After many washing with deionized water over time, the resultant combination was finally diluted with alcohol. The resulting precipitates were dried at 120 °C as a consequence. Er-doped nanoparticles of CeO₂ were synthesized and heated at 400 °C for 4 h since the power obtained from warmth can enhance oscillations and transfer of lattice-like elements during crystallization. The exact test

methods were used to produce Barium-doped CeO₂ using barium nitrate hexahydrate (Khadar et al., 2019; Masui et al., 1997).

1.2. Antibacterial activity

Bacterial cultures containing *Bacillus subtilis*, *Staphylococcus aureus*, *E. coli*, and *P. aeruginosa*, among others, were acquired from the Eumic Analytic Lab and Research Institute in Tiruchirappalli. Bacterial strains were cultivated on nutrient agar slants (Hi medium) at 4 °C. Bacterial cultures were subculture in a liquid medium (nutrient broth) at 37 degrees Celsius for 8 h before being tested for 10⁵–10⁶ CFU/ML. All of these suspensions were made shortly before the examination was performed. Nutrient agar medium is one of the most used media for a variety of regular bacteriological applications. After combining all of the components with the filtered water, it is heated to completely disintegrate the medium and then autoclaved at 15 psi pressure (121 °C) for 15 min. The nutritional broth was made using the same ingredients except agar. The nutrient broth was made, and identified bacterial colonies were added to the broth and cultivated for antimicrobial

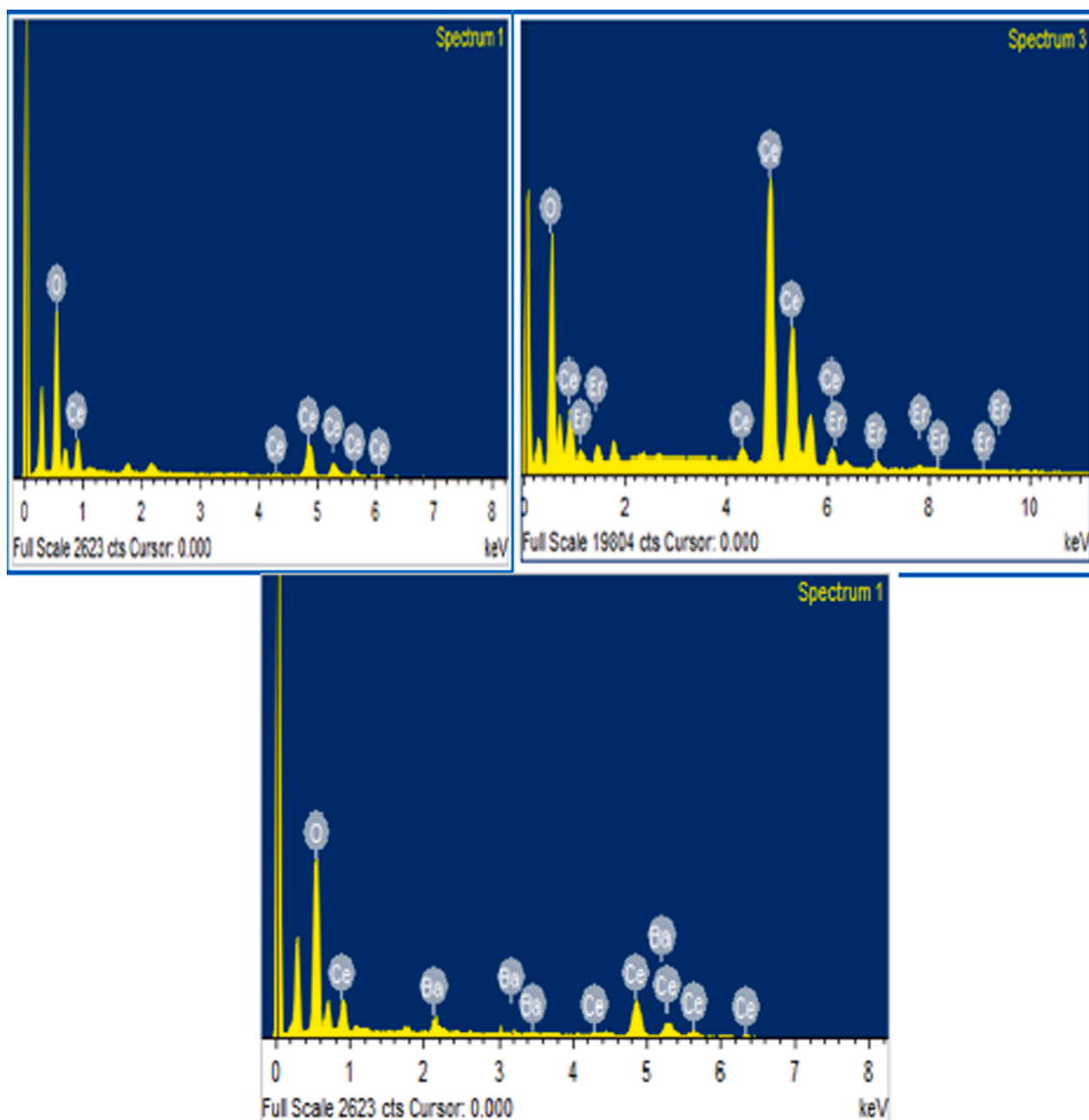


Fig. 3. EDX profile of (a) Pristine CeO_2 (b) Er doped CeO_2 (c) Ba doped CeO_2 NPs.

properties. The nutritional agar solution was produced and sterilized by steam sterilization at 121°C and 15 lb of pressure for fifteen minutes before aseptically pouring it into sterile petri plates and allowing it to harden. The bacterial broth culture was swabbed on each petri plate with clean buds. The wells were then dug by a well cutter. Pure and doped CeO_2 has been added to every sample aseptically. This method was repeated for each petri-plate which was subsequently incubated at 37°C for 24 h. Following the incubation process the glass plates were examined for the zone of inhibition.

1.3. Analytical characterization

The granule specimens have been examined for phase makeup and quantity employing an X-ray diffractometer (Bruker D8 Advance) with $\text{CuK}\alpha$ radiation and a Bruker Lynx Eye detector. PANalytical, Netherlands, was also employed for the exact same objective, utilizing a 3 kW X-ray tube with a copper objective as the radiation source and real-time multiple-strip solid-state detectors equipped with graphite crystals for K beta screening. X-ray spectra have been obtained from 5 to 50. The results of the XRD were processed to identify the crystallized components. The surface morphology and crystallographic orientation of the

samples were investigated using scanning electron microscopy and an energy-dispersive X-ray spectrometer. SEM photos were captured with the model JEOL-JSM-35 LF, which has a voltage range of 5–35 kilo Volts of KV and a resolution of 5000 X. and the size of Nanoparticles can be accurately measured from SEM images using image J analysis software with proper calibration and measurement techniques. Fourier transform infrared spectroscopy (FTIR, Bruker Optic GmbH, Tensor 27, Germany) was used to identify the functional groups in the produced samples. 1 % of the powder was combined with 99 % KBr and formed into pellets with a diameter of 3 mm at 5 MPa/torr, which was then examined in the $400\text{--}4000\text{ cm}^{-1}$ area. A UV-visible photometer (Shimadzu, Model UV-1800) was used to measure the optical characteristics of nanoparticles of metal oxide in the 200–850 nm spectrum, with a resolution of 1 nm. Photo luminescence has been determined utilizing a luminescence spectrophotometer (Perkin Elmer, Model: LS-5513, USA) using a xenon lamp as the excitation source at ambient temperature.

Table 1

Percentage of composition elements presents in as-fabricated pristine CeO₂ and Er and Ba doped CeO₂ NPs.

S.NO	MATERIAL	(%) Composition of Elements			
		Ce	O	Er	Ba
1	Pristine CeO ₂	79.45 %	20.55 %	–	–
2	Ba doped CeO ₂	75.40 %	3.92 %	–	20.68 %
3	Er doped CeO ₂	70.73 %	4.15 %	25.12 %	–

2. Results and discussion

2.1. XRD finding

The crystalline state of produced pure CeO₂ Er and Ba-doped CeO₂ nanoparticles was observed using XRD analysis. Fig. 1 (a-c) depicts the XRD criteria for the produced pure and doped CeO₂. The ceria nanoparticles are a common calcium fluoride crystal form with the space group Fm3m (Abbas et al., 2015; Azad et al., 2005). The XRD pattern shows well-set peaks for (111), (200), (220), (311), (222), (400), (311), and (420) at 2θ values = 28.68°, 33.23°, 47.45°, 56.45°, 59.39°, 69.49°, 76.77°, and 79.02°, indicating a cubic fluorite structure for CeO₂

(Fig. 1 a-c). This is also supported by JCPDS data (card no. 00–34-0394) (Khulbe et al., 2020; Pinna et al., 2012). Furthermore, no XRD patterns of any other group phase were discovered as impurities, showing that the substituted along with untreated particles are very pure and crystalline (Fig. 1 a-c). In comparison to the pure CeO₂ sample, the Barium and Erbium doped CeO₂ nanoparticles shows no significant change in diffraction peak values. The change reflects the amount of distortion caused by the substitution of Ba and Er ions with Ce ions in each compound owing to the ionic radius of the specific metal ions, which occurs at boiling heat. The mean size of ordered pure CeO₂ nanoparticles is given using Debye-Scherrer's formula, as shown following (Pinna et al., 2020).

$$D = 0.9 \lambda / \beta \cos \theta \quad (1)$$

In this equation, D- represents Crystallite size, λ-is the wavelength of the radiation (1.5406 Å for CuKα), k is a constant (0.94), β- is Full Width Half Maximum (FWHM), and θ is the peak location. It was discovered that the average crystallite diameter of pure CeO₂ nanoparticles is 25 nm. The average crystallite size increases in Ba and Er-CeO₂ nanoparticles reached 74 nm and 40 nm, correspondingly. Increase in particle size observed may be due to the increase in calcination humidity. This increase in humidity could potentially lead to a reduction in particle size during the calcination process (Pop et al., 2020).

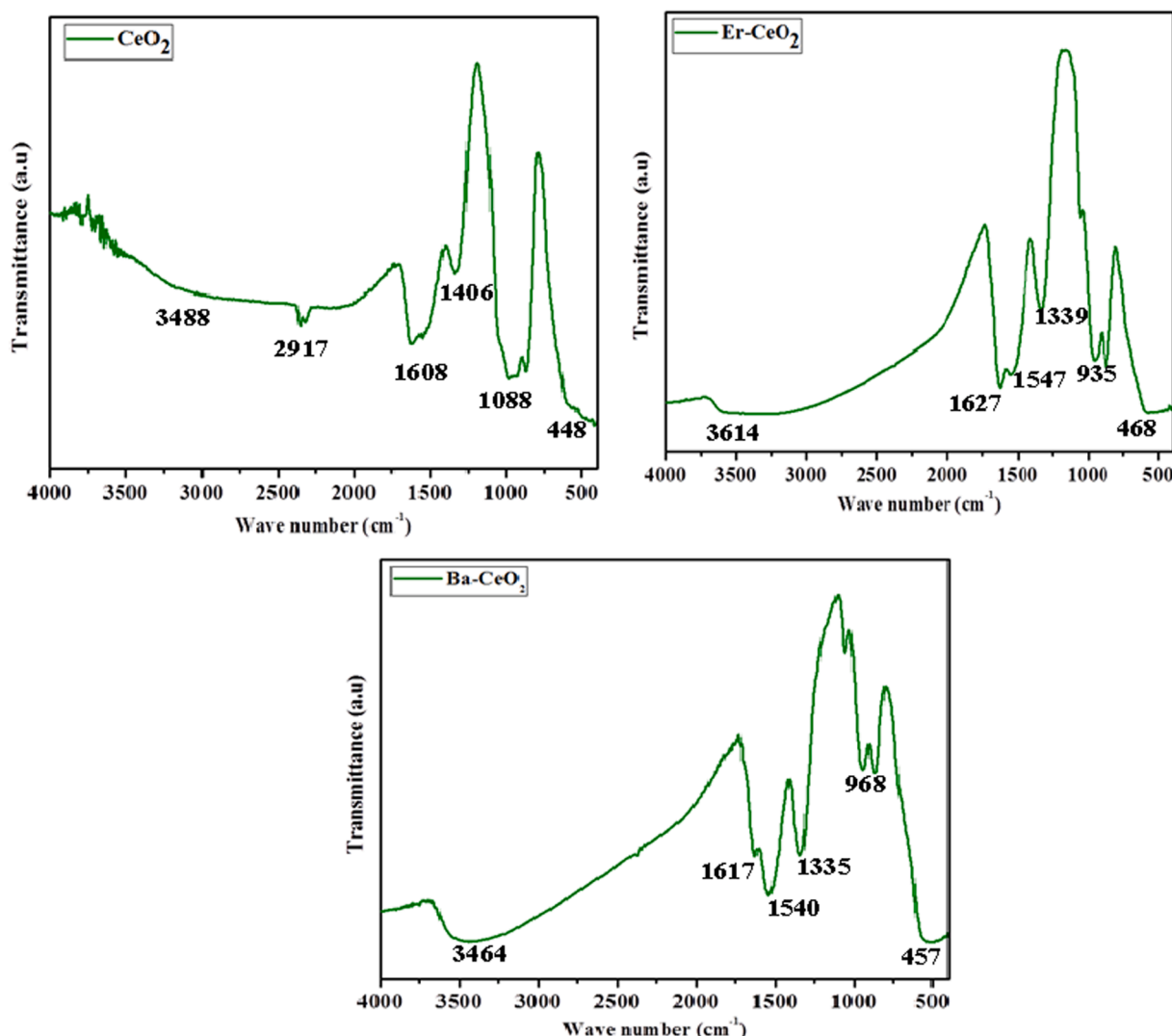


Fig. 4. FT IR spectrum of (a) Pristine CeO₂ (b) Er doped CeO₂ (c) Ba doped CeO₂ NPs.

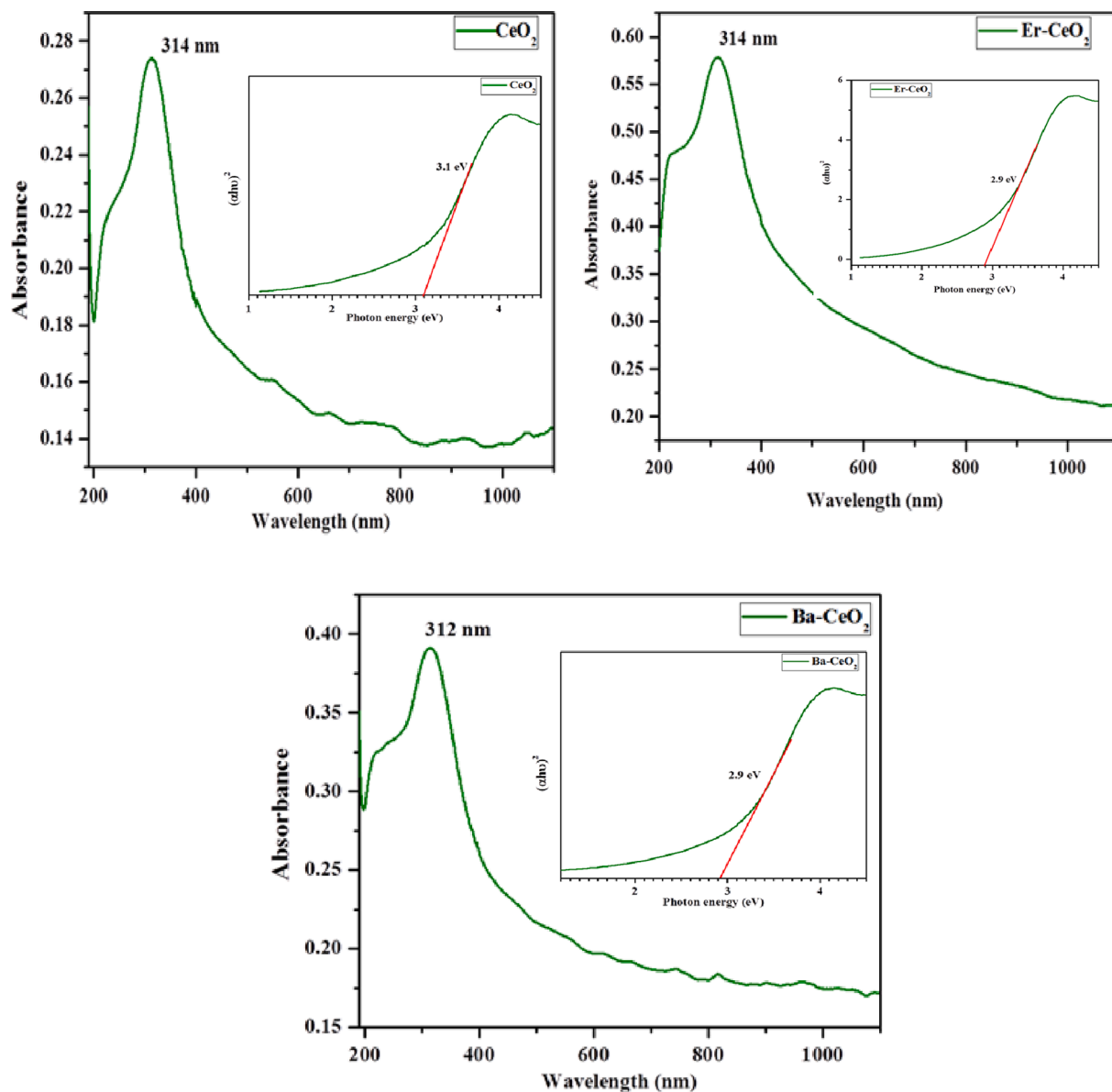


Fig. 5. UV-Visible optical spectrum (a) Pristine CeO_2 (b) Er doped CeO_2 (c) Ba doped CeO_2 NPs and (inset) band gap of Pristine CeO_2 , Ba and Er doped CeO_2 NPs.

2.2. SEM morphological analyses

Fig. 2 illustration (a–c) shows micrographs obtained using SEM of pure CeO_2 , Ba, and Er- CeO_2 nanoparticles. The size of nanoparticles was calculated using image J software. The annealed nanoparticles between 350 and 400 °C were homogeneous in size, ranging from 20 to 30 nm for CeO_2 and 35 to 75 nm for Ba and Er- CeO_2 . The typical widths of cubic particles for pure CeO_2 , Ba, and Er doped CeO_2 particles are 26, 75, and 41 nm, respectively. Interestingly, the high-magnification SEM micrographs (Fig. 2(b)) have an irregular spherical form consistent with the literature, however, the corresponding Fig. 2(c) shows a nanowire-like structure instead of a spherical form. The reaction circumstances determine the difference between the two dopant topologies. According to this viewpoint, nanoparticles may exhibit mild aggregation due to inadequate annealing temperature and a lack of sonication. The average particle sizes of clean and modified nanoparticles match those calculated from XRD measurements (Mahalakshmi et al., 2024).

2.3. EDX studies

The presence of doped rare earth metals on the ceria crystal surface was confirmed by its atomic weight percentage, which was determined utilizing EDAX. Fig. 3 (a–c) shows the EDAX spectra of pure CeO_2 and CeO_2 nanoparticles loaded with Er or Ba. Percentage of composition elements represents in Table 1.

2.4. FT-IR findings

The IR spectra of pure CeO_2 , Ba, and Er-doped CeO_2 nanoparticles are given in Fig. 4 (a–c). For Er and Ba-doped CeO_2 , the bands at 3614 and 3464 cm^{-1} corresponds to the –OH groups, whereas the highest frequencies at 1621 and 1617 cm^{-1} correspond to the H–O–H twisting resonance of weakly charged or absorption water. The peak at 1339 cm^{-1} and 1335 cm^{-1} is due to the vibrational form of nitro compounds. The asymmetric stretching vibrations of COO were detected at 1547 cm^{-1} and 1540 cm^{-1} . The distinctive metallic oxide movement, Er–O–Er and Ba–O–Ba, might be responsible for both of the major peaks at 479 cm^{-1} and 968 cm^{-1} for Er- CeO_2 and peaks at 457 cm^{-1} and 935 cm^{-1} for

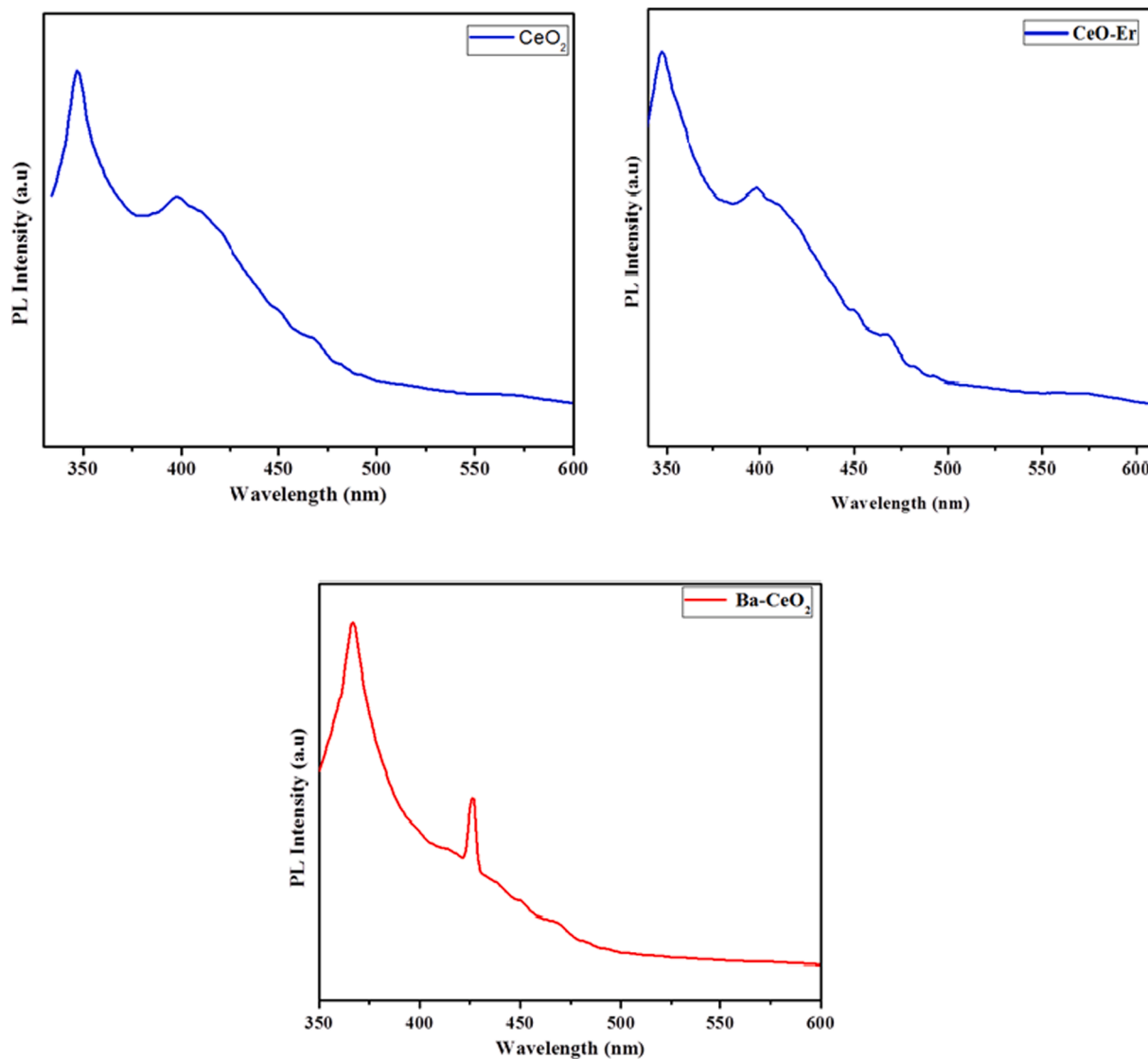


Fig. 6. Photoluminescence spectrum (a) Pristine CeO₂ (b) Er doped CeO₂ (c) Ba doped CeO₂ NPs.

Ba- CeO₂ in the IR spectra (Badi'ah et al., 2019; Parimi et al., 2019).

2.5. Uv-visible spectroscopic investigations

Fig. 5 (a-c) depicts the UV-visible absorption spectrum of pure CeO₂, Er, and Ba-doped CeO₂ nanoparticles calcined at 400 °C. The stimulation maximum for pure nanoparticles of CeO₂ was approximately 314 nm, whereas Er and Ba-doped CeO₂ nanoparticles had wavelengths of excitation in the 314 & 312 nm spectrum ranges, as illustrated in Fig. 5 (b-c). The absorption spectrum of Er and Ba-doped CeO₂ nanoparticles shifted to the longer frequency side when contrasted with pure CeO₂ particles. This means that the band gap of CeO₂ nanoparticles reduces when Er and Ba bonds develop with oxide at CeO₂ grid sites. The optical band gap energy of Er and Ba-doped CeO₂ nanoparticles is computed using the usual Tauc relationship (Nurhasanah et al., 2018; Habib et al., 2018).

$$(ah\nu)^{1/n} = A(h\nu - E_g) \quad (2)$$

Where, A – is a stable, n varies with the change, and E_g – represents the gap in the optical band. The value of n = 1/2, 3/2, 2, or 3 (order) varies according to the kind of electrical transfer. The sixth illustration (a-c) depicts a plot of (αhν)² vs photon energy (hν) for Er and Ba-doped CeO₂ nanoparticles after boiling at 400 degrees Celsius, taking into account

the explicit group transitions. Extrapolating the linear area of these figures to (αhν)² = 0 yields the corresponding photon energy. The optical band gap energy of pure CeO₂ nanoparticles is 3.1 eV, while Er and Ba-doped CeO₂ nanoparticles have 2.8 eV. When matching the Er and Ba treated eV findings to CeO₂ nanoparticles, the abrupt decrease in the band gap or red shift may be explained by the bottom of the Burstein-Moss (BM) effect, although the Fermi level changes occurred extremely close to the conduction band owing to the rise in transport density. The small transition of energy is forbidden and the frequency value gap narrows due to the amalgamation of Er and Ba ions in the CeO₂ crystal lattice. No additional broadband emission is seen due to the reformation transition from the 4f band of Ce⁴⁺ ions to the valence band or the 5d-4f transition of Ce³⁺ ions (Sharma et al., 2020; Gopinath et al., 2015).

2.6. Photoluminescence research

Fig. 6 (a-c) Photoluminescence spectrum shows the emission spectra of pure CeO₂ nanoparticles and Ba, Er-doped CeO₂ nanoparticles, with an excitation wavelength of 312 & 314 nm compared to the absorption spectra data. The pure CeO₂ nanoparticles display a significant emission spike at 348 nm; it is attributed to the passage of protons through the confined Ce_{4f} state to the O_{2p} of the valence band. Furthermore, a peak

Table 2

Zone of inhibition of pure and doped CeO₂ nanoparticles against bacterial strains tested.

Organisms	100 μ L DMSO Extract added and zone of inhibition (mm)			
	<i>Bacillus subtilis</i>	<i>Staphylococcus aureus</i>	<i>E. Coli</i>	<i>Pseudomonas aeruginosa</i>
CeO ₂	18	14	10	12
Ba-CeO ₂	20	16	12	15
Er-CeO ₂	16	12	18	15
DMSO	—	—	—	—
Tetracycline	25	15	20	25

of radiation seen at 396 nm was caused by defective conditions that existed broadly between Ce_{4f} states and the O_{2p} of the valence band. Furthermore, the emission of CeO₂:Er nanoparticles progressively reduced by concerning 399 nm as well as continued to a maximum of 494 nm. The localized Ce_{4f} state to O_{2p} of the valence band in CeO₂:Er nanoparticles is associated with emission, which gradually reduces in the CeO₂ crystal structure owing to Er ion doping. Furthermore, the emission band was gradually enlarged from 427 nm to 453 nm, and it was prolonged up to 471 nm for CeO₂ and Ba nanoparticles. At the same time, the emission nature was red-shifted due to lower defect levels generated by Er and Ba ions. As a result, the intensity of emission of the CeO₂ in the surroundings gradually decreased, owing to the formation of more oxygen defects or increases in surface defects, as well as the restraint of electron transfer from Ce_{4f} to O_{2p} levels as the content of doping increased (Mohan et al., 2021; Deepa et al., 2022).

2.7. Antibacterial activity

The antibacterial activity of pure CeO₂ and doped nanoparticles containing CeO₂ was tested against the Gram-negative microbes *E. coli* and *P. aeruginosa*, in addition to the Gram-positive bacteria *B. subtilis* and *S. aureus*. Table 2 compares the antibacterial activity of pure CeO₂ and doped nanoparticles of CeO₂ against this bacterium. The aforementioned research shows that CeO₂ and doped CeO₂ nanoparticles are

efficient in inhibiting a certain variety of bacterial growth. Fig. 8 shows the antibacterial activity of CeO₂ and doped CeO₂ nanoparticles against *E. coli*, *P. aeruginosa*, *B. subtilis*, and *S. aureus* using ZOI. The zone of inhibition (ZOI) of around 18 and 14 mm for CeO₂, 20 mm and 16 mm for Ba-CeO₂, and 16 and 12 mm for Er-CeO₂ were observed for the Gram-positive bacteria strain *B. subtilis* and *S. aureus* (American Type Culture Collection 25923), and Fig. 7 display the determined ZOI for the Gram-negative bacteria strain *E. coli* and *P. aeruginosa* (American Type Culture Collection 25922) were 10 mm and 12 mm for CeO₂, 12 mm and 15 mm for Ba-CeO₂, and 18 and 15 mm for Er. Given these findings, it can be inferred that the produced pure CeO₂ and doped CeO₂ nanoparticles had a significant antibacterial impact on both Grade categories of bacteria. Pure CeO₂ and doped CeO₂ nanoparticles have better antibacterial action against Gram-positive bacteria (especially *B. subtilis*) than Gram-negative microbes, Er-CeO₂ in the case of *E. coli*. The variation in activities among these two species of bacteria might be linked to variances in cell membrane structure and composition (Agarwal et al., 2018; Cedervall et al., 2007). The CeO₂ nanoparticles were shown to have antibacterial action because they can produce reactive oxygen species that can damage cells of bacteria. In this regard, several processes have been proposed to explain metal oxides' antibacterial properties. Bacterial susceptibility to O-CeO₂ nanoparticles varies depending on particle size, synthesis temperature, bacterial cell wall structure, and degree of interaction with nanoparticle-containing organisms. Furthermore, the increased susceptibility of the two types of bacteria to CeO₂ nanoparticles has been linked to the higher number of nitro and carboxyl groups on their cell walls, which increases the affinity of Ce ions for these groups. Smaller nanoparticle sizes and CeO₂ nanoparticles generated at lower temperatures showed superior antibacterial activities in our present study. In this investigation, Gram-positive *B. subtilis* showed a greater inhibition zone than Gram-negative isolates used in the bacterial sensitivity test (Sudhakaran et al., 2023).

2.7.1. Bactericidal mechanism

It is possible that pure CeO₂, Er and Ba doped CeO₂ NPs could play a role in the redox transformation of Ce ions once they reach the cell walls

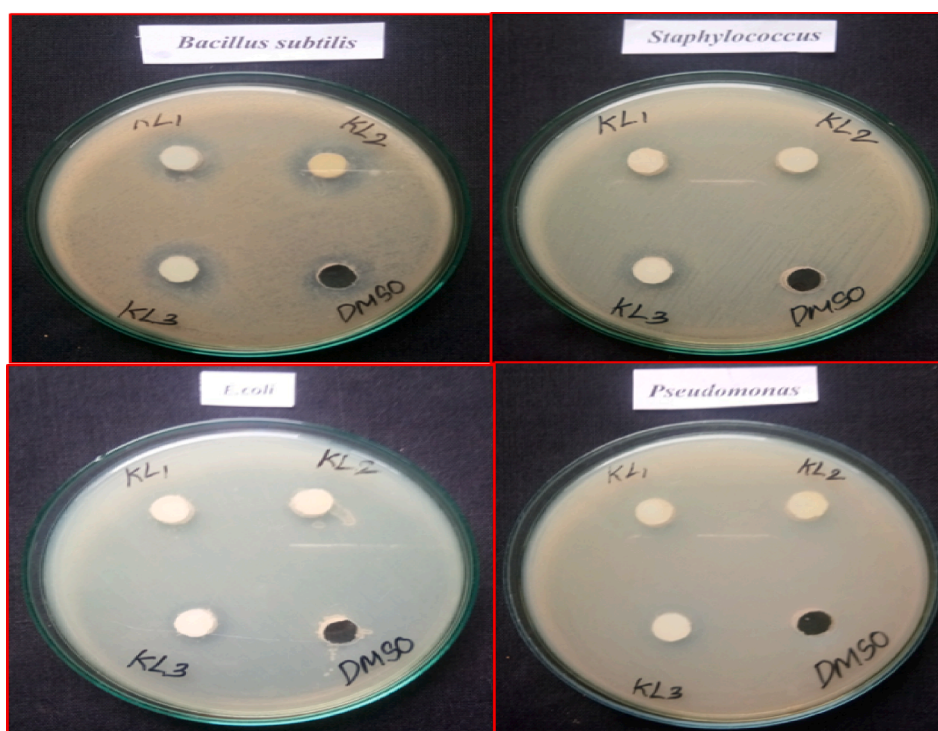


Fig. 7. Bactericidal properties of pristine CeO₂ NPs and Ba doped CeO₂ NPs by co-precipitation approach.

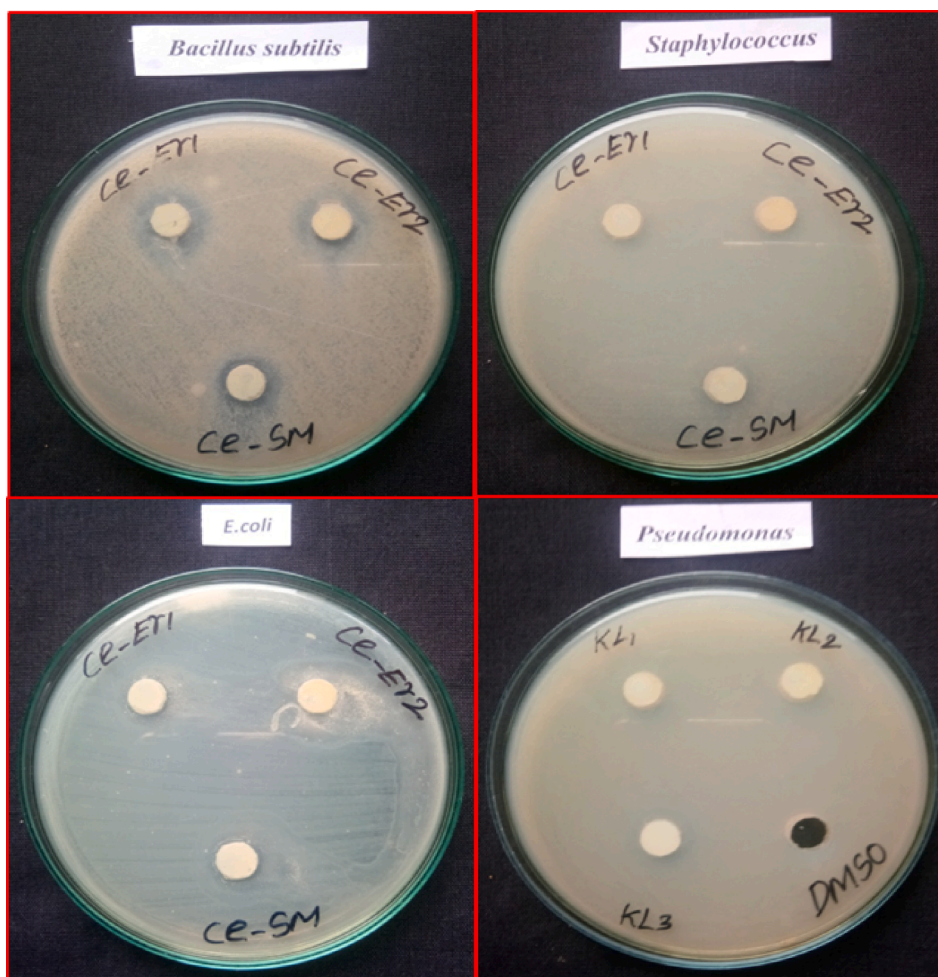


Fig. 8. Bactericidal properties of pristine CeO₂ NPs and Er doped CeO₂ NPs by Co-precipitation approach.

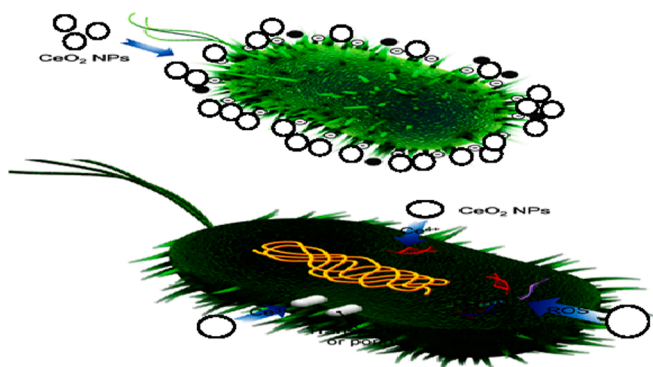


Fig. 9. Bactericidal mechanism of pure CeO₂, Er and Ba doped CeO₂ NPs.

of bacteria. Depending on the conditions within the cell, Ce⁴⁺ atoms may reduce to Ce³⁺ or inversely. For most cases, what keeps the Ce³⁺ to Ce⁴⁺ ratio constant is CeO₂ (IV) + e⁻ → CeO₂(III) (Azzam and Zaki, 2016). The process that leads to enhanced antibacterial effectiveness is demonstrated in Fig. 9. Certain oxidizing agents, such as free radicals (OH^{*}, H₂O₂, and O₂^{*}), possess the ability to cross the barrier formed by bacteria and cause damage by interfering with its permeability. The conversion of Ce⁴⁺ to Ce³⁺ also increases reactive oxygen species (ROS) generation. Both stresses caused by oxidative stress as well as the oxidation of lipids contribute to ROS-induced microbial cell extinction. Strong reactive oxygen species (ROS) have the potential to harm several

bacterial ingredients, such as amino acids, mitochondrion and DNA. Because of this, the bacterial cell becomes damaged, and the microbes eventually die (Chatterjee et al., 2011; Pitchumani Krishnaveni and Annadurai, 2019; Pozharitskaya et al., 2020).

3. Conclusion

The present study successfully developed small fragments composed of cerium oxide and cerium dioxide injected with doped elements Er and Ba using an affordable precipitation method. X-ray diffraction analysis revealed a cubic fluorite layout for the nanocrystals, while SEM images showed irregularly shaped nanoparticles ranging from 20 to 30 nm. Infrared spectra indicated the presence of Er and Ba oxides or hydroxide compounds in the particles, with optical band gap energies of 3.2 eV in pure CeO₂ and 2.9 eV in doped CeO₂ NPs. The addition of Er and Ba ions resulted in a redshift in frequency gap, with a strong emission peak at 348 nm in pure CeO₂ nanoparticles. Additionally, the antimicrobial tolerance experiment showed a larger inhibiting area for the Gram-positive *B. subtilis* strain compared to other Gram-negative isolates. Overall, these findings demonstrate the potential applications of these doped nanoparticles in various fields.

CRediT authorship contribution statement

K. Loganathan: Conceptualization, Formal analysis, Resources, Software. **R.P. Suresh Jeyakumar:** Conceptualization, Data curation, Formal analysis. **Natarajan Arumugam:** Conceptualization, Data curation, Project administration, Software, Supervision, Validation,

Writing – review & editing. **Sinouvasane Djearmane:** Resources, Supervision, Validation, Writing – review & editing. **Ling Shing Wong:** Conceptualization, Supervision, Validation, Visualization. **Saminathan Kayarohanam:** Data curation, Funding acquisition, Project administration, Software, Validation, Writing – review & editing.

Acknowledgement

The project was funded by Researchers Supporting Project number (RSP2024R143), King Saud University, Riyadh, Saudi Arabia. In addition to one of the authors Dr. K. Loganathan is thankful to the DST-FIST, New Delhi (SR/FST/COLLEGE/2022/1290) and the Principal of Vivekanandha College of Arts and Sciences for Women (Autonomous) for providing necessary facilities.

References

- Abbas, F., Jan, T., Iqbal, J., Ahmad, I., Naqvi, M.S., Malik, M., 2015. Facile synthesis of ferromagnetic Ni doped CeO₂ nanoparticles with enhanced anticancer activity. *Appl. Surf. Sci.* 357, 931–936.
- Agarwal, H., Menon, S., Kumar, S.V., Rajeshkumar, S., 2018. Mechanistic study on antibacterial action of zinc oxide nanoparticles synthesized using green route. *Chem. Biol. Interact.* 286, 60–70.
- Alpaslan, E., Gellich, B.M., Yazici, H., Webster, T.J., 2017. PH-controlled cerium oxide nanoparticle inhibition of both gram-positive and gram-negative bacteria growth. *Sci. Rep.* 7, 1–12.
- Azad, A.M., Matthews, T., Swary, J., 2005. Processing and characterization of electrospun Y₂O₃-stabilized ZrO₂ (YSZ) and Gd₂O₃-doped CeO₂ (GDC) nanofibers. *Mater. Sci. Eng. B* 123 (3), 252–258.
- Azzam, E.M., Zaki, M.F., 2016. Surface and antibacterial activity of synthesized nonionic surfactant assembled on metal nanoparticles. *Egypt. J. Pet.* 25 (2), 153–159.
- Badi'ah HI, Seede F, Supriyanto G, Zaidan AH (2019) Synthesis of silver nanoparticles and the development in analysis method. In IOP Conf. Ser.: Earth Environ. Sci. 217, No. 1, p. 012005. IOP Publishing.
- Cedervall T, Lynch I, Lindman S, Berggård T, Thulin E, Nilsson H, Dawson KA, Linse S. (2007) Understanding the nanoparticle–protein corona using methods to quantify exchange rates and affinities of proteins for nanoparticles. *Proceedings of the National Academy of Sciences.* 104(7):2050-5.
- Chatterjee, S., Bandyopadhyay, A., Sarkar, K., 2011. Effect of iron oxide and gold nanoparticles on bacterial growth leading towards biological application. *J. Nanobiotechnol.* 9 (1), 1–7.
- Cuahtecantzi-Delint, R., Mendez-Rojas, M.A., Bandala, E.R., Quiroz, M.A., Recillas, S., Sanchez-Salas, J.L., 2013. Enhanced antibacterial activity of CeO₂ nanoparticles by surfactants. *Int. J. Chem. React. Eng.* 11, 781–785.
- Deepa, T., Mohan, S., Manimaran, P., 2022. A crucial role of selenium nanoparticles for future perspectives. *Results in Chemistry* 4, 100367.
- Farias, I.A.P., Dos Santos, C.C.L., Sampaio, F.C., 2018. Antimicrobial activity of cerium oxide nanoparticles on opportunistic microorganisms: A systematic review. *Biomed Res. Int.* p. 1923606
- Gopinath, K., Karthika, V., Sundaravadevelan, C., Gowri, S., Arumugam, A., 2015. Mycogenesis of cerium oxide nanoparticles using *Aspergillus niger* culture filtrate and their applications for antibacterial and larvicidal activities. *Journal of Nanostructure in Chemistry.* 5 (3), 295–303.
- Habib, I.Y., Kumara, N.T., Lim, C.M., Mahadi, A.H., 2018. Dynamic light scattering and zeta potential studies of ceria nanoparticles. In: *InSolid State Phenomena*, Vol. 278. Trans Tech Publications Ltd., pp. 112–120
- Khadar, Y.A.S., Balamurugan, A., Devarajan, V.P., Subramanian, R., Kumar, S.D., 2019. Synthesis, characterization and antibacterial activity of cobalt doped cerium oxide (CeO₂: Co) nanoparticles by using hydrothermal method. *J. Mater. Res. Technol.* 8, 267–274.
- Khadar, Y.S., Balamurugan, A., Devarajan, V.P., Subramanian, R., Kumar, S.D., 2019. Synthesis, characterization and antibacterial activity of cobalt doped cerium oxide (CeO₂: Co) nanoparticles by using hydrothermal method. *J. Mater. Res. Technol.* 8 (1), 267–274.
- Khulbe, K., Karmakar, K., Ghosh, S., Chandra, K., Chakravorty, D., Muges, G., 2020. Nanoceria-based phospholipase-mimetic cell membrane disruptive antibiofilm agents. *ACS App. Bio. Mater.* 3 (7), 4316–4328.
- Kumar, S., Gautam, S., Song, T.K., Chae, K.H., Jang, K.W., Kim, S.S., 2014. Electronic structure study of Co doped CeO₂ nanoparticles using X-ray absorption fine structure spectroscopy. *J. Alloy. Compd.* 611, 329–334.
- Kumar, S., Ahmed, F., Shaalan, N.M., Saber, O., 2021. Biosynthesis of ceo2 nanoparticles using egg white and their antibacterial and antibiofilm properties on clinical isolates. *Crystals* 11, 584.
- Mahalakshmi, G., Elangovan, K., Mohan, S., Arumugam, N., Almansour, A.I., 2024. Bio-reticulation of Pd nanorods enables catalytic treatment of various cloth dyes. *Applied Nanoscience* 1–12.
- Mallesappa, J., Nagabhushana, H., Sharma, S.C., Vidya, Y.S., Anantharaju, K.S., Prashantha, S.C., Prasad, B.D., Naika, H.R., Lingaraju, K., Surendra, B.S., 2015. *Leucas aspera* mediated multifunctional CeO₂ nanoparticles: structural, Photoluminescent, Photocatalytic and Antibacterial properties. *Spectrochim. ACTA Part A Mol. Biomol. Spectrosc* 149, 452–462.
- Masui, T., Fujiwara, K., Machida, K.I., Adachi, G.Y., Sakata, T., Mori, H., 1997. Characterization of cerium (IV) oxide ultrafine particles prepared using reversed micelles. *Chem. Mater.* 9 (10), 2197–2204.
- Mohan, S., Devan, M.V., Sambathkumar, S., Shanmugam, V., Ravikumar, K., 2021. Dual probes of Ag/Pd bimetallic NPs facilely synthesized by green process using *Catharanthus* leaf extract on textile dye removal and free radical capability. *Applied Nanoscience* 11, 1565–1574.
- Nithya, P., Sundrarajan, M., 2020. Ionic liquid functionalized biogenic synthesis of AgeAu bimetal doped CeO₂ nanoparticles from *Justicia adhatoda* for pharmaceutical applications: Antibacterial and anti-cancer activities. *J. Photochem. Photobiol. B Biol.* 202, 111706.
- Nurhasanah I, Safitri W, Arifin Z, Subagio A, Windarti T. (2018) Antioxidant activity and dose enhancement factor of CeO₂ nanoparticles synthesized by precipitation method. *InIOP Conference Series: Materials Science and Engineering* (Vol. 432, No. 1, p. 012031). IOP Publishing.
- Parimi, D., Sundararajan, V., Sadak, O., Gunasekaran, S., Mohideen, S.S., Sundaramurthy, A., 2019. Synthesis of positively and negatively charged CeO₂ nanoparticles: investigation of the role of surface charge on growth and development of *Drosophila melanogaster*. *ACS Omega* 4 (1), 104–113.
- Pelletier, D.A., Suresh, A.K., Holton, G.A., McKeown, C.K., Wang, W., Gu, B., Mortensen, N.P., Allison, D.P., Joy, D.C., Allison, M.R., et al., 2010. Effects of engineered cerium oxide nanoparticles on bacterial growth and viability. *Appl. Environ. Microbiol.* 76, 7981–7989.
- Pinna, A., Figus, C., Lasio, B., Piccinini, M., Malfatti, L., Innocenzi, P., 2012. Release of ceria nanoparticles grafted on hybrid organic–inorganic films for biomedical application. *ACS Appl. Mater. Interfaces* 4 (8), 3916–3922.
- Pinna, A., Cali, E., Kerherve, G., Galleri, G., Maggini, M., Innocenzi, P., Malfatti, L., 2020. Fulleropyrrolidine-functionalized ceria nanoparticles as a tethered dual nanosystem with improved antioxidant properties. *Nanoscale Advances.* 2 (6), 2387–2396.
- Pitchumani Krishnaveni, M., Annadurai, G., 2019. Biosynthesis of nanoceria from *Bacillus subtilis*: characterization and antioxidant potential. *Res. J. Life Sci.* 5 (3), 644.
- Pop, O.L., Mesaros, A., Vodnar, D.C., Suharschi, R., Tăbăran, F., Mageruşan, L., Tódor, I. S., Diaconeasa, Z., Balint, A., Ciontea, L., Socaci, C., 2020. Cerium oxide nanoparticles and their efficient antibacterial application in vitro against gram-positive and gram-negative pathogens. *Nanomaterials* 10 (8), 1614.
- Pozharitskaya, O.N., Obluchinskaya, E.D., Shikov, A.N., 2020. Mechanisms of bioactivities of fucoidan from the brown seaweed *Fucus vesiculosus* L. of the Barents Sea. *Mar. Drugs* 18(5):275.
- Sharma, G., Prema, D., Venkataprasanna, K.S., Prakash, J., Sahabuddin, S., Venkatasubbu, G.D., 2020. Photo induced antibacterial activity of CeO₂/GO against wound pathogens. *Arab. J. Chem.* 13 (11), 7680–7694.
- Sudhakaran, R., Deepa, T., Babu, S., Mohan, S., 2023. New developed for generating superhydrophobic surface modification on mild steel for corrosion protection. *Results in Chemistry* 5, 100968.